J. Magn. Soc. Jpn., **40**, 67-70 (2016)

<Paper>

Iron Loss Calculation for Concentric-Winding Type Three-Phase Variable Inductor based on Reluctance Network Analysis

Kenji Nakamura, Yuta Yamada, Takashi Ohinata*, Kenji Arimatsu*,
Takehiko Kojima**, Makoto Yamada**, Ryohei Matsumoto**,
Masaya Takiguchi**, and Osamu Ichinokura
Graduate School of Engineering, Tohoku University, *6-6-05 Aoba Aramaki Aoba-ku, Sendai 980-8579, Japan*
*Tohoku Electric Power Co., Inc., *1-7-1 Honcho Aoba-ku, Sendai 980-8550, Japan*
**Fuji Electric Co., Inc., *1-11-2 Osaki Shinagawa-ku, Tokyo 141-0032, Japan*

A variable inductor consisting of just a magnetic core and primary dc and secondary ac windings, is able to control effective inductance of the secondary ac winding linearly and continuously by the primary dc current due to magnetic saturation effect. Therefore, it can be applied as a var compensator in electric power systems. The variable inductor has desirable features such as simple and robust structure, low cost, and high reliability. In a previous paper, a novel concentric-winding type three-phase variable inductor was proposed. It was demonstrated in experiments that the proposed variable inductor has good controllability and low distortion current. This paper presents a method for calculating iron loss of the proposed variable inductor based on reluctance network analysis (RNA). The validity of the proposed method is demonstrated through a comparison with measured values.

Key words: three-phase variable inductor, concentric-winding, iron loss, reluctance network analysis (RNA)

1. Introduction

In electric power systems, line voltage stabilization is one of the important subjects because renewable and distributed power sources such as wind-turbine and photovoltaic power generations are being introduced in large quantities. In order to regulate the line voltage, the semiconductor power converters such as a static var compensator (SVC) and a static synchronous compensator (STATCOM) have been introduced [1), 2)]. These apparatuses, however, have some problems including harmonic current, electromagnetic interference (EMI), and high cost.

A variable inductor consists of only a magnetic core and primary dc and secondary ac windings [3)], but can control effective inductance of the secondary ac winding linearly and continuously by the primary dc current due to magnetic saturation effect. Thus, it can be used as a var compensator by combining with a power capacitor [4)]. The variable inductor has simple and robust structure, high reliability, and low cost. These features are advantages for applications in electric power systems. Several kinds of variable inductors have been proposed. However, all the previously proposed variable inductors have a single-phase structure. Hence, at least three variable inductors are required for the var compensation in electric power systems.

To resolve the above problem, a three-phase variable inductor was presented in a previous paper [5)]. It has only one laminated-core in which three-phase secondary ac windings are installed together. The previous three-phase variable inductor demonstrated good controllability and low distortion current, but the winding space factor was low since the primary dc windings must be placed on the ring yoke.

To improve the winding space factor, a novel concentric-winding type three-phase variable inductor was proposed [6), 7)]. It has primary dc and secondary ac windings which are concentrically wound on each leg. It was indicated that the reactive power per weight of the proposed variable inductor is about 1.6 times larger than that of the previous one, namely, the weight of the proposed variable inductor can be reduced by 40% [8)].

This paper presents an iron loss calculation of the proposed variable inductor based on reluctance network analysis (RNA). The establishment of the iron loss calculation method is indispensable for the optimum design of the var compensator. The usefulness of the proposed method is proved by comparing with measured values.

2. Basic configuration and operating principle of concentric-winding type three-phase variable inductor

Fig. 1 illustrates a basic configuration of a concentric-winding type three-phase variable inductor, which consists of six legs, two ring yokes, and primary dc

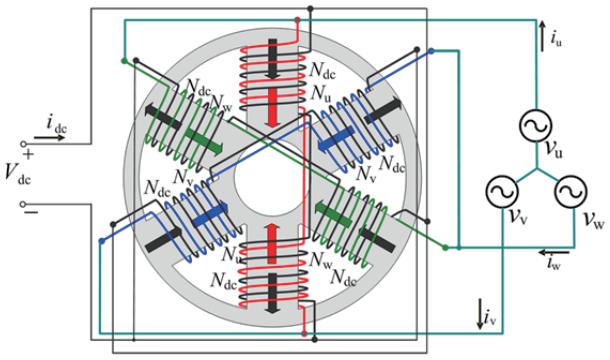

Fig. 1. Basic configuration of a concentric-winding type three-phase variable inductor.

and secondary ac windings. The secondary ac windings N_u, N_v, N_w are coiled around each couple of legs on the straight line, respectively. These windings are connected in delta, and to the three-phase ac voltage source. On the other hand, each primary dc winding N_{dc} is concentrically wound on the leg where the secondary ac winding is coiled around, and a couple of the primary dc windings on the straight line is connected in series to cancel the induced voltages caused by the secondary ac fluxes.

3. Iron loss calculation for concentric-winding type three-phase variable inductor

Fig. 2 shows the specifications of a trial 4.0 kVA concentric-winding type three-phase variable inductor. The core material is non-oriented silicon steel with a thickness of 0.35 mm. The number of turns of the primary dc winding N_{dc} is 114, and the secondary ac windings N_u, N_v, N_w are 208 each. The rated capacity and voltage are 4.0 kVA and 200 V so that it can be handled in the laboratory. Fig. 3 indicates an appearance of the trial concentric-winding type three-phase variable inductor.

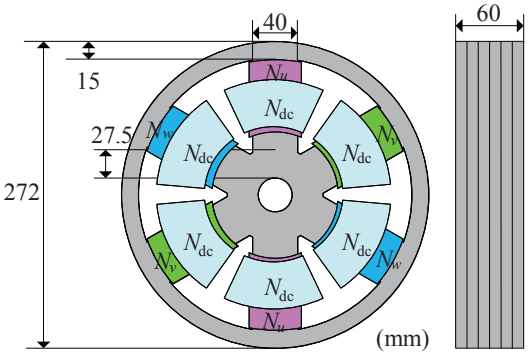

Rated capacity	4.0 kVA
Rated voltage	200 V
Frequency	50 Hz
Primary dc winding: N_{dc}	114 turns x 6, 0.164 Ω/coil
Secondary ac winding: N_u, N_v, N_w	208 turns x 6, 0.604 Ω/coil
Winding space factor	43.9%
Core material	NGO with 0.35 mm

Fig. 2. Specifications of a trial 4.0 kVA concentric-winding type three-phase variable inductor.

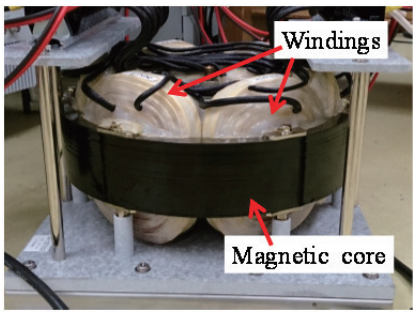

Fig. 3. Appearance of the trial 4.0 kVA concentric-winding type three-phase variable inductor.

To calculate the iron loss of the variable inductor, three-dimensional (3-D) RNA is employed because its analytical model is simple, the calculation speed and accuracy are high, and the coupled analysis is readily performed.

First, the three-phase laminated-core is divided into multiple elements as shown in Fig. 4(a). To take leakage flux into consideration, the surrounding space of the core is also divided. The divided elements can be expressed in a 3-D unit magnetic circuit shown in Fig. 4(b). When the 3-D unit magnetic circuit is in the core region, the reluctances R_{mr} and $R_{m\theta}$ express the magnetic nonlinearity, and the magnetic inductances R'_r and R'_θ represent the iron loss of the core. These elements can be obtained as follows.

When considering the iron loss, a relationship between the magnetic field H and the flux density B can be given by [9]

$$H = \alpha_1 B + \alpha_m B^m + \beta_1 \frac{dB}{dt} + \beta_n \left(\frac{dB}{dt}\right)^n . \qquad (1)$$

The first and second terms of (1) denote the magnetic nonlinearity, and the third and fourth terms express the iron loss.

The coefficients α_1 and α_m are determined by a B-H curve of core material shown in Fig. 5(a), while the coefficients β_1 and β_n are obtained from a core loss curve shown in Fig. 5(b), which includes hysteresis and eddy current losses in the core. These coefficients are m = 13, α_1 = 106, α_{13} = 6.3, n = 9, β_1 = 0.14, and β_9 = 2.0×10^{-26}, respectively.

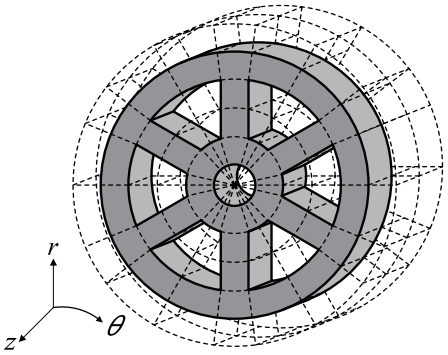

(a) Core division

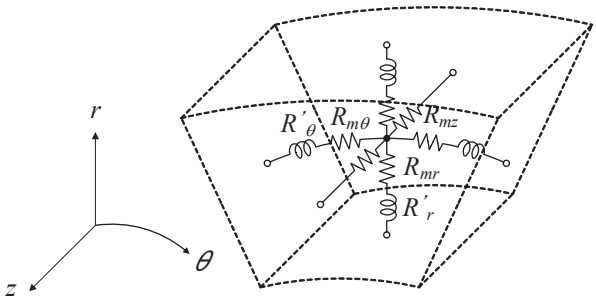

(b) 3D unit magnetic circuit

Fig. 4. Three-dimensional RNA model of the three-phase laminated-core.

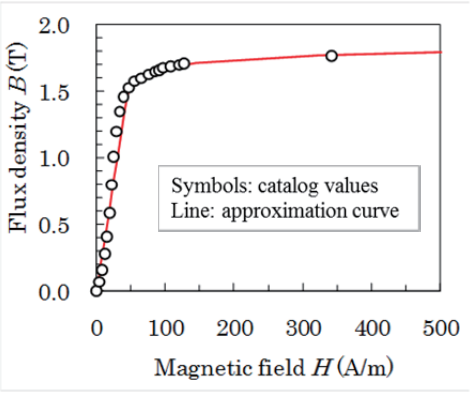

(a) *B-H* curve

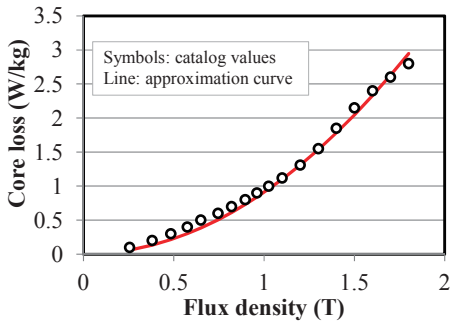

(b) Core loss curve

Fig. 5. *B-H* curve and core loss curve of the core material.

From (1), a relationship between the magnetomotive force (MMF) f and the flux ϕ is given by

$$f = Hl$$

$$= R_m\phi + R'\frac{d\phi}{dt}$$

$$= \left(\frac{\alpha_1 l}{S} + \frac{\alpha_m l}{S^m}\phi^{m-1}\right)\phi + \left\{\frac{\beta_1 l}{S} + \frac{\beta_n l}{S^n}\left(\frac{d\phi}{dt}\right)^{n-1}\right\}\frac{d\phi}{dt}, \quad (2)$$

where the magnetic path length and the cross section of each divided element are l and S, respectively. The reluctances and the magnetic inductances in the 3-D unit magnetic circuit can be determined by (2).

On the other hand, the reluctance R_{mz} in the z-axis direction should be determined considering a laminated structure of the core. Apparent permeability in the z-axis μ_e is given by

$$\frac{1}{\mu_e} = \frac{d_f}{\mu_s} + \frac{1-d_f}{\mu_0}$$

$$\cong \frac{1-d_f}{\mu_0}, \quad (3)$$

where the vacuum and core permeability are μ_0 and μ_s, and the space factor of the laminated silicon steel core is d_f, respectively. Accordingly, R_{mz} is obtained as a linear reluctance from (3).

On the other hand, when the unit magnetic circuit is in the surrounding space, the linear reluctances R_{mr}, $R_{m\theta}$, R_{mz} are obtained from the dimensions of each divided element and the vacuum permeability μ_0, while the magnetic inductances R'_r, R'_θ are zero.

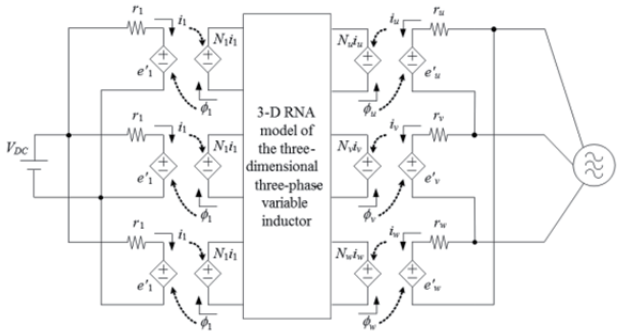

Fig. 6. Electric- and magnetic-coupled model of the concentric-winding type three-phase variable inductor.

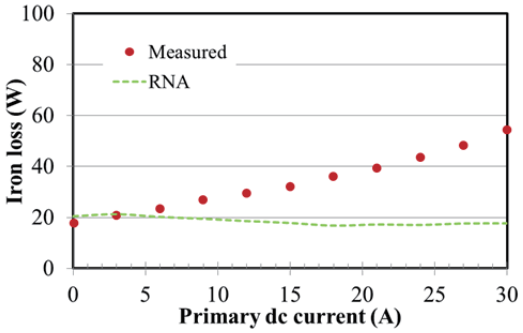

Fig. 7. Measured and calculated iron losses of the concentric-winding type three-phase variable inductor.

Finally, when the RNA model obtained in the way described above is coupled with the external electric circuits as shown in Fig. 6, the characteristics of the variable inductor can be calculated by a general purpose circuit simulator SPICE [10].

Fig. 7 shows the measured and calculated iron losses of the concentric-winding type three-phase variable inductor. Both values are in good agreement when a primary dc current is 0 A. Contrary to this, the error increases as the primary dc current becomes large. The reason is that the RNA model shown in Fig. 4 is able to consider only the iron loss caused by the flux flowing in the r- and θ-directions, which is parallel with the laminated silicon steel. On the other hand, the eddy current loss caused by the leakage flux flowing in the z-axis direction, which is perpendicular to the laminated silicon steel, is neglected

4. RNA model considering eddy currents on laminated silicon steel

In general, the eddy currents on the laminated silicon steel are distributed in a complicated manner. To take this into consideration in RNA, the following assumption is applied [11]: The distribution of the eddy currents is based on the division of the RNA model as shown in Fig. 8, and the eddy current flows uniformly in each element.

To express the eddy current on the laminated silicon steel in the RNA model, the 3-D unit magnetic circuit and the eddy current circuit are combined as shown in Fig. 9. In the figure, the leakage flux ϕ_z gives the induced

voltage e_z. From the induced voltage e_z and the resistance R_{ed}, the eddy current i_{ed} can be obtained, which gives the MMF in the 3-D unit magnetic circuit. In practice, all the eddy current circuits are connected with each other as shown in Fig. 10 to consider the current interaction between the adjacent elements.

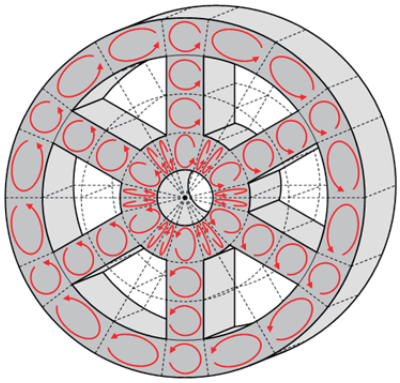

Fig. 8. Distribution of the eddy currents in the RNA model.

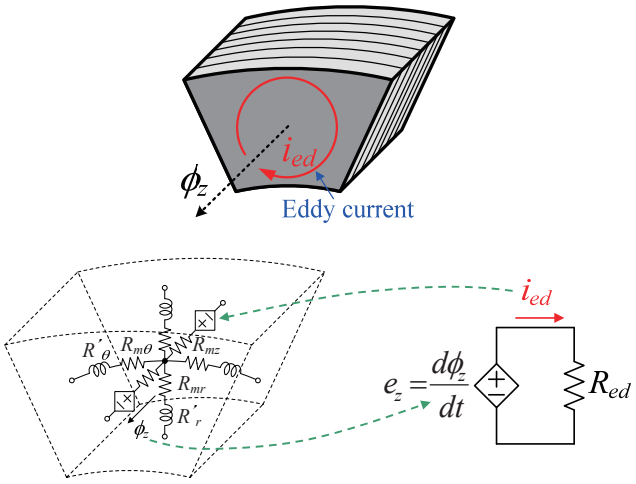

Fig. 9. 3-D unit magnetic circuit combined with the eddy current circuit.

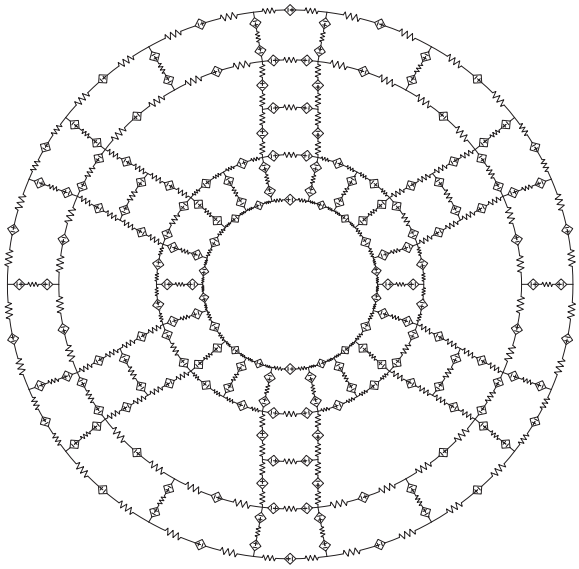

Fig. 10. Eddy current network model.

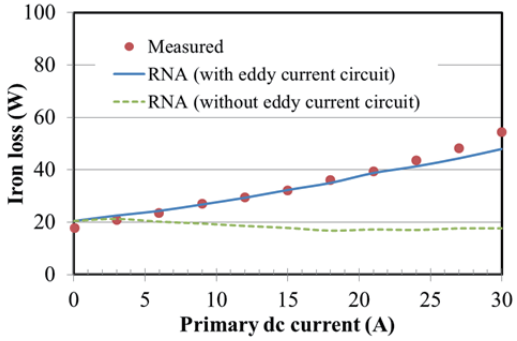

Fig. 11. Comparison of the measured and calculated iron losses of the concentric-winding type three-phase variable inductor.

Fig. 11 shows the comparison of the measured and calculated iron losses of the concentric-winding type three-phase variable inductor. In the figure, the symbols show the measured values and the solid line indicates the calculated ones. In addition, the broken line represents the calculated values when the eddy current on the laminated silicon steel is ignored. The figure clearly indicates that the calculated values agree well with the measured ones.

5. Conclusion

This paper presented a method for calculating iron loss of the concentric-winding type three-phase variable inductor based on RNA.

It was clear that the eddy currents on the laminated silicon steel must be considered in order to estimate the iron loss of the concentric-winding type three-phase variable inductor. The usefulness of the proposed method was proved by comparing with the measured values.

References

1) L. Gyugyi, *IEEE Trans. Ind. Applicat.*, **IA-15**, 521 (1979).
2) S. Mori, K. Matsuno, T. Hasegawa, S. Ohnishi, M. Takeda, M. Seto, S. Murakami, and F. Ishiguro, *IEEE Trans. Power Sys.*, **8**, 371 (1993).
3) S. D. Wanlass, C. L. Wanlass, and L. K. Wanlass, *IEEE Wescon Tech. Papers*, **12**, part 2 (1968).
4) O. Ichinokura , T. Tajima, and T. Jinzenji, *IEEE Trans. Magn.*, **29**, 3225 (1993).
5) K. Nakamura, S. Hisada, K. Arimatsu, T. Ohinata, K. Sakamoto, and O. Ichinokura, *IEEE Trans. Magn.*, **44**, 4107 (2008).
6) K. Nakamura, K. Honma, T. Ohinata, K. Arimatsu, T. Shirasaki, and O. Ichinokura, *J. Magn. Soc. Jpn.*, **38**, 174 (2014).
7) K. Nakamura, K. Honma, T. Ohinata, K. Arimatsu, and O. Ichinokura, *Journal of Applied Physics*, **117**, 17D523 (2015).
8) K. Nakamura, K. Honma, T. Ohinata, K. Arimatsu, T. Kojima, M. Yamada, R. Matsumoto, M. Takiguchi, and O. Ichinokura, *IEEE Trans. Magnetics*, **51**, 8402104 (2015).
9) K. Tajima, O. Ichinokura, A. Kaga, and Y. Anazawa, *J. Magn. Soc. Jpn.*, **19**, 553 (1995) (in Japanese).
10) K. Tajima, A. Kaga, and O. Ichinokura, *T. IEE Japan*, **117-A**, 155 (1997) (in Japanese).
11) K. Nakamura, T. Tomonaga, S. Akatsuka, T. Ohinata, K. Minazawa, and O. Ichinokura, *J. Magn. Soc. Jpn.*, **30**, 273 (2006).

Received Nov. 25, 2015; Accepted Feb. 23, 2016